عملية الكسر لفولاذ الكربون – المنجنيز (C – Mn) الهش بالهيدروجين

نور الدين سعيداني، عبدالقادر ميحي، رشيد بن بوتة

قسم الميكانيك، كلية التكنولوجيا، جامعة باتنة، باتنة 05000، الجزائر

الملخص:

تم فحص بنية عينات تكسرت عن طريق اختبار إجهاد الشد بسرعة تشوه بطيئة، بهدف دراسة أصناف الكسر (التقصف) باستخدام مجهر مسح إلكتروني.

أرشدت هذه الدراسة إلى تحديد ثلاثة أصناف من العينات: عينات غير هشة، عينات خفيفة الهشاشة وعينات هشة جدا. وتتألف الفئة الأولى من عينات الاختبار التي تمت تجربتها في الهواء بجهد −0.80 و −0.85 فولط. وذلك بسبب هشاشة ≤ 0.97 كما تم اختبار العينات خفيفة الهشاشة بجهد −0.90 فولط مع معدل الهش 0.69. أما بالنسبة للعينات المعنية بنسبة الهش أقل من 0.69 فتدخل في الفئة ذات العينات الهشة جدا.

أثبتت دراسات صور الانكسار أن هش الفولاذ الصلب ناتج عن الهش بواسطة الهيدروجين. كما لوحظ أن البنية (بين الحبيبات وعبر الحبيبات) لمقاطع الانكسار، بالنسبة للفولاذ الهش، هي نموذجية ودالة الهش بالهيدروجين.

Journal of the Association of Arab Universities for Basic and Applied Sciences (2012) **11**, 16–20

University of Bahrain

Journal of the Association of Arab Universities for Basic and Applied Sciences

www.elsevier.com/locate/jaaubas
www.sciencedirect.com

ORIGINAL ARTICLE

Fracture process of C–Mn steel embrittled by hydrogen

N. Saidani, A. Mihi, R. Benbouta *

University of Batna, Faculty of Technology, Mechanical Engineering Department, Batna 05000, Algeria

Available online 31 January 2012

KEYWORDS

Fracture;
Hydrogen embrittlement;
Morphologies;
Fracture modes;
Scanning electron microcopy (SEM)

Abstract Fracture morphologies of tested specimens, by means of the slow strain rate tensile testing, were examined to study fracture modes by using scanning electron microscopy.

This study has led to the determination of three categories of specimens: unembrittled specimens, slightly embrittled specimens and severely embrittled specimens. The first category of unembrittled specimens includes specimens tested in air, at potentials of −0.80 and −0.85 V (SCE) with embrittlement ratio (ER) $\geqslant 0.97$. In the category of specimens slightly embrittled, only the specimen tested at −0.9 V with an embrittlement ratio (ER) of 0.69 is included. The last category of severely embrittled specimens includes the specimens with embrittlement ratio (ER) < 0.69.

The fractographic studies are consistent with the embrittlement of steel being due to hydrogen embrittlement. The intergranular and transgranular quasicleavage fracture surface morphologies observed with embrittled specimens are typical and characteristic of hydrogen embrittlement.

1. Introduction

The detrimental effect which hydrogen produces in metals, generally known as hydrogen embrittlement (HE), has always been one of the main problems of practical and theoretical material technology of corrosion and protection of metals.

Hydrogen is the cause of damage whenever metal hydrogen systems are involved in the production, transport and storage of hydrogen, or fluids containing hydrogen, and in the presence of electrochemical processes such as pickling, electroplating, cathodic protection and corrosion. Hydrogen when present either as an external gas environment or as a dissolved proton can produce internal cracking or a dramatic loss of toughness in a variety of metals (Takeda and McMahon, 1981; Gooch, 1974; Woodward and Procter, 1988; Hirth and Johnson, 1976; Luu and Wu, 2001; Wu and Wu, 2002).

When considering the hydrogen embrittlement phenomenon, one of the areas that is of most interest is the mode of hydrogen fracture.

In the present work the objective was to study the fracture process of the specimens tested under slow strain rate testing (SSRT).

2. Experimental procedure

2.1. Material

The material investigated in the present study was low carbon-manganese structural steel BS 4360 grade 50D. The nominal composition of this material and its mechanical properties in the condition in which it has been tested are given in Table 1. The cylindrical tensile specimens with a 25.0 mm gauge length

* Corresponding author. Tel./fax: +213 0 33 81 21 43.
E-mail address: r_benbouta@yahoo.fr (R. Benbouta).

Peer review under responsibility of University of Bahrain.
doi:10.1016/j.jaubas.2012.01.001

ELSEVIER **Production and hosting by Elsevier**

Table 1 Mechanical properties and chemical composition of steel.

Mechanical properties	Heat treatment
$\sigma_{0.2}$ = 1220 MPa	Austenitization for 1 min at 1200 °C
U.T.S = 1440 MPa	Water quench
RA = 48%	Tempered for 30 min at 170 °C

Chemical composition wt%

C	Si	Mn	S	P	Ni	Cr	Mo
0.16	0.34	1.44	0.011	0.026	0.03	0.06	< 0.02

and 3.0 mm gauge diameter were obtained in a longitudinal direction from rolled plate steel. Prior to testing, the specimens were ground longitudinally using 180, 400, 600 and 800 grit emery papers, ultrasonically cleaned in methanol, rinsed in deionized water and dried in warm air. Apart from the gage length, the specimens were then coated with ''lacomit''.

2.2. Experimental details

2.2.1. Slow strain rate testing

2.2.1.1. Test apparatus. The apparatus for the SSRT is similar to an ordinary tension testing machine, but the drive mechanism produces much slower crosshead speeds than those encountered in a tension test. In brief, it consists of a fixed frame, a carriage, a drive mechanism, a load cell and recorder, using an electric-synchronous motor and a suitable gear reducer. The carriage can be pulled downward at a constant rate in the range of 10^{-7}–10^{-4} mm/s. Thus, the downward movement of the carriage pulls the specimen in tension to fracture.

2.2.1.2. Slow strain rate tests. Specimens were subject to conventional, monotonic slow strain rate tensile testing in laboratory air and in 3.5% NaCl solution, without precharging, at cathodic potentials of −0.8, −0.85, −0.9, −0.95, −1.0, −1.1 and −1.2 V. All tests were conducted at room temperature and in natural aerated conditions. A potentiostat was used to control the potential of the specimen during the test. The potential of the specimen was measured relative to a saturated calomel electrode (SCE). A strain rate of $2.077 \times 10^{-7}\ s^{-1}$ was mainly used throughout.

2.2.1.3. Assessment of SSRT results. Measurement of specimen ductility in slow strain rate test provides a convenient parameter for hydrogen embrittlement susceptibility. Elongation, reduction of area (RA) or embrittlement ratio (ER) can be used. The last two parameters were adopted and calculated as follows:

$$\mathrm{RA}(\%) = \frac{A_0 - A}{A_0} 100\%$$

Where: A is the area of the fractured surface, and A_0 is the original area prior to straining.

$$\mathrm{ER} = \frac{\mathrm{RA(Test\ Environment)}}{\mathrm{RA(Air)}}$$

2.3. Fractography

Examination of the fracture surface and side surface of each studied specimen was performed using a Hitachi H-45 scanning electron microscope (SEM). The voltage used during examination was 20 KV.

3. Results

3.1. Electron fractography of tensile specimens

3.1.1. Fracture in air

SEM fractography of the steel tested in air showed that the specimen fractured in a pattern of microvoid coalescence (MVC). Fig. 1 shows fractograph of specimen failed in air. It can be seen that the tensile specimen ruptured at the neck in a cup and cone fracture appearance which tended to initiate at the central region of the specimen. The deformation pattern developed below the fracture surface indicates that this kind of ductile fracture mode involves a large amount of plastic deformation before final failure. A typical fractograph of equiaxed

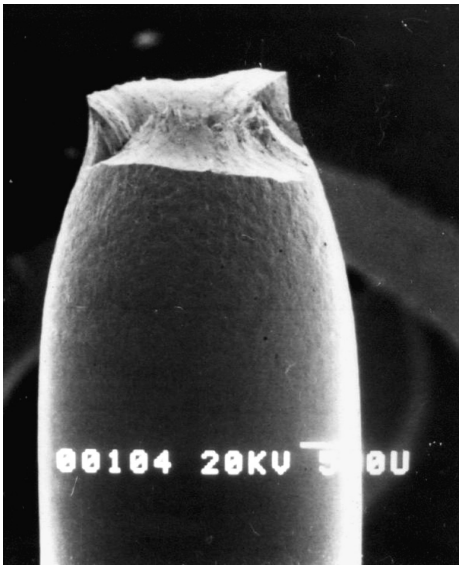

Figure 1 SEM photomicrograph of fractured specimen tested in air.

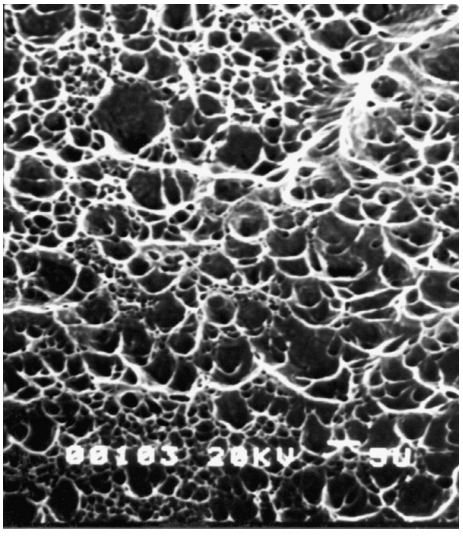

Figure 2 Typical photomicrograph of equiaxed dimples.

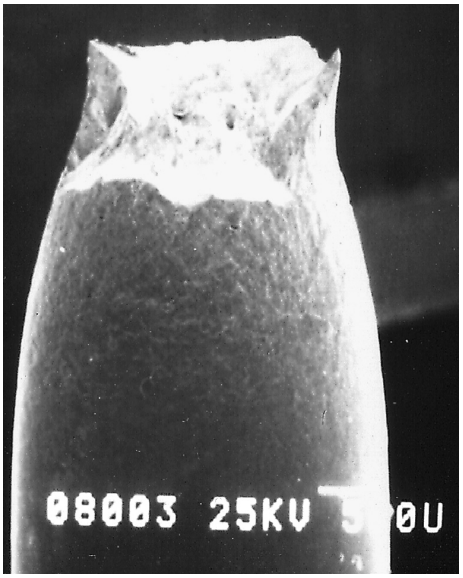

Figure 3 SEM photomicrograph of fractured specimen tested at −0.85 V (SCE).

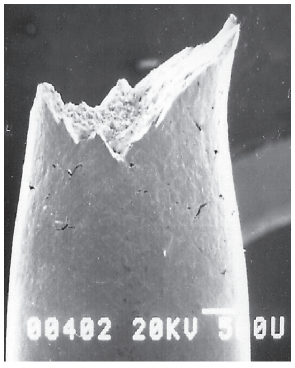

(a) Gauge section

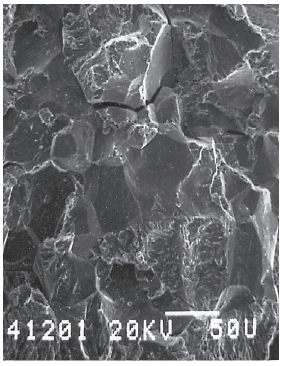

(b) Fracture surface edge

Figure 4 SEM photomicrographs of the gauge section and fracture surface edge of steel at −0.9 V (SCE).

dimples contained in the central cup of the fracture surfaces is shown in Fig. 2. These dimples are the result of the growth and coalescence of microvoids which nucleate at particles such as inclusions and precipitates.

3.1.2. Fracture in 3.5% NaCl

3.1.2.1. Tests at −0.8 and −0.85 V. For the tests performed at −0.8 and −0.85 V the fracture surface of specimens had also a cup and cone appearance similar to that obtained in the air test, Fig. 3.

3.1.2.2. Test at −0.9 V. In this test, some embrittlement was noticed. Failure occurred with an amount of plastic deformation lower than that observed in tests in air, and at −0.8 and −0.85 V, Fig. 4a. The fracture surface consisted of a ragged fracture path and smoother fracture path inclined at about 45° from the loading direction. A few patches, consisted predominantly of intergranular cracking along the prior austenite grain boundaries, were observed at the edge of the ragged fracture path. A photomicrograph of the brittle area is shown in Fig. 4b.

3.1.2.3. Tests at −0.95 to −1.3 V. The tests carried out at potentials of −0.95 to −1.3 V showed high degree of embrittlement (ER ranged from 0.063 to 0.323). Examination of the fracture surfaces indicated similarities between the fracture morphologies. The fracture surfaces appeared to have a flat fracture profile normal to the loading direction and shear type fracture oriented at about 45° to the tensile axis. Typical photomicrographs of fracture are shown in Fig. 5.

In general, the fracture surfaces consisted mainly of a large ductile region and small brittle area. The brittle area was generally localized at or near the edge of the fracture surface with a predominantly intergranular cracking along the prior austenite grain boundaries and limited areas of quasicleavage. Fig. 6 is characteristic of the features observed on many fracture surfaces in this potential range. It was noticed that as the potential became more negative the proportion of the brittle region increases.

4. Discussion

4.1. Fracture process

4.1.1. Unembrittled specimens

All these specimens fractured in a similar pattern of microvoids coalescence. Usually, the microvoids nucleate at regions of highly localized plastic deformation such as inclusions and grain boundaries. As the stress on the specimen increases, the microvoids expand and intersect one another and finally break up when the reduced cross sectional area cannot withstand the load any longer.

4.2. Slightly embrittled specimens

In this case, brittle type of failure, predominantly intergranular cracking along prior austenite grain boundaries and some quasicleavage features, accompanied the ductile type of failure such as dimples and ductile tearing. The proportion of the brittle region was minimal, only one or two patches localized at the edges of the specimen. It is believed that the presence and growth of these brittle types of fracture cause the cross section of the specimen, already reduced by necking, to be reduced even more, and thus, the specimen will fail earlier than in their absence. Because of the limited amount of hydrogen available under these conditions, the cracks do not grow long enough to cause an earlier reduction in the net cross sectional area.

4.3. Severely embrittled specimens

In this category of tests, the hydrogen availability is very high, it diffuses into steel through the lattice and accumulates at defect sites such as dislocations, inclusions, grain boundaries, microvoids, phase interface and carbides. Its interaction with certain of these defects results in intergranular or transgranular quasicleavage cracking. Since the availability of hydrogen is high, the number of sites for crack nucleation increases and they grow long enough so that they could link more easily, resulting in a surface covered with a large fraction of brittle types of failures. Also, as the cracks grow faster, the reduction in the net cross sectional area occurs at an earlier stage than when insufficient hydrogen is available.

In summary the reduced ductility of the C–Mn structural steel when tested in NaCl solution at cathodic applied

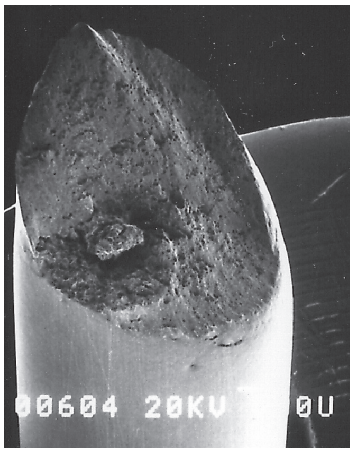

(a) Gauge section (- 1. 1 V)

(b) Fracture surface(- 1. 1 V)

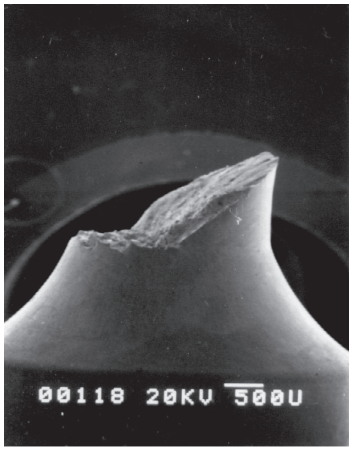

(c) Gauge section (- 1.3 V)

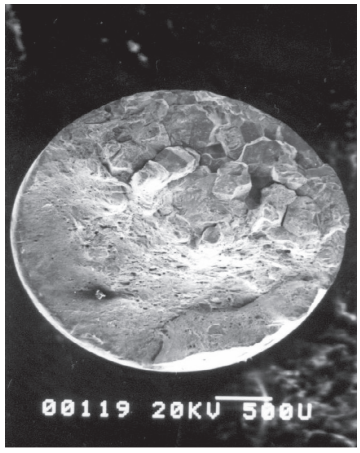

(d) Fracture surface(- 1.3 V)

Figure 5 Typical SEM photomicrographs of the gauge sections and fracture surfaces of specimens tested at potentials between −0.95 and −1.3 V (SCE).

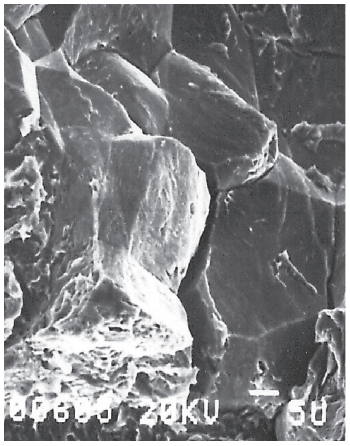

(a) Tested at –0.95 V

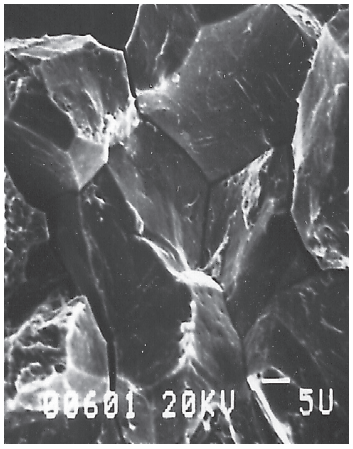

(b) Tested at – 1.1 V

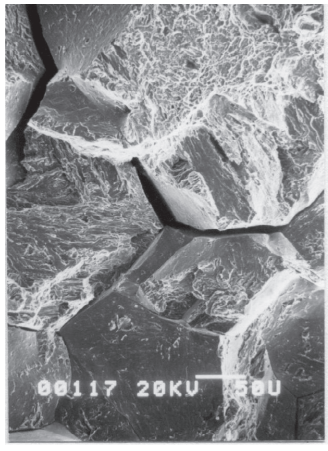

(c) Tested at – 1.3 V

Figure 6 Selected SEM photomicrographs of the fracture surface edge of specimens tested at potentials between −0.95 and −1.3 V (SCE).

potentials is the result of the presence of mainly intergranular cracks induced by cathodically evolved hydrogen. The hydrogen which has diffused through the lattice accumulates at susceptible interfaces, and probably lowers the cohesive strength of the lattice after a critical concentration has been reached, thereby initiating an embrittling event at room temperatures in ductile steel (Yoshino and McMahon, 1974; Wang et al., 2007).

5. Conclusion

This work is devoted to fractographic investigation of C–Mn structural steel under slow strain rate tensile testing. Examination of the fracture surfaces using SEM revealed the following results:

1. The intergranular and transgranular quasicleavage fracture surface morphologies observed with embrittled specimens are typical and characteristic of hydrogen embrittlement.
2. The reduction in ductility of steel is attributed to the appearance of brittle modes of fracture such as intergranular and transgranular quasicleavage features on the fracture surface.

References

Gooch, T.G., 1974. Stress corrosion cracking of welded joints in high strength steels weld. Welding Journal 53, 2877.

Hirth, J.P., Johnson, H.H., 1976. Hydrogen problems in energy related technology. Corrosion 32, 3.

Luu, W.C., Wu, J.K., 2001. Influence of aluminium content on retarding hydrogen transport in Fe–Al binary alloys. Corrosion Science 43, 2325.

Takeda, Y., McMahon, C.J., 1981. Strain controlled vs stress controlled hydrogen induced fracture in a quenched and tempered steel. Metallurgical Transactions 12A, 1255.

Wang, M., Akiyama, E., Tsuzaki, K., 2007. Effect of hydrogen on the fracture behavior of high strength steel during slow strain rate test. Corrosion Science 49, 4081.

Woodward, J., Procter, R.P.M., 1988. Fatigue of offshore structures. In: Dover, W.D., Glinka, G. (Eds.), Proceedings of International Conference, London.

Wu, T.I., Wu, J.K., 2002. Effects of thiourea and its derivatives on the electrolytic hydrogenation behavior of Ti–6Al–4V alloy. Materials Letters 53, 193.

Yoshino, K., McMahon Jr., 1974. The cooperative relation between temper embrittlement and hydrogen embrittlement in a high strength steel. Metallurgical Transactions 5A, 363.